pH-dependent, extended release and enhanced *in vitro* efficiency against colon cancer of Tegafur formulated using chitosan-coated poly (ε-caprolactone) nanoparticles

Ana Medina-Moreno [a], Mazen M. El-Hammadi [b], José L. Arias [a,c,d,*]

[a] *Department of Pharmacy and Pharmaceutical Technology, Faculty of Pharmacy, University of Granada, 18071, Granada, Spain*
[b] *Department of Pharmacy and Pharmaceutical Technology, Faculty of Pharmacy, University of Seville, 41012, Sevilla, Spain*
[c] *Institute of Biopathology and Regenerative Medicine (IBIMER), Center of Biomedical Research (CIBM), University of Granada, 18100, Granada, Spain*
[d] *Biosanitary Research Institute of Granada (ibs.GRANADA), Andalusian Health Service (SAS), University of Granada, 18071, Granada, Spain*

ABSTRACT

Tegafur is used to treat various malignant lesions, including advanced gastric and colorectal cancers. However, its efficacy is limited by its low oral bioavailability, short half-life and serious toxicity. To address these drawbacks, a nanoformulation of poly(ε-caprolactone) nanoparticles coated with chitosan was developed for the delivery of Tegafur. Poly(ε-caprolactone) particles were prepared by an interfacial polymer disposition method, while surface functionalization with chitosan followed a coacervation procedure. Transmission electron microscopy and elemental analyses, and electrokinetics of the particles demonstrated that such core/shell nanostructure was obtained. Compared to unmodified particles, chitosan-coated nanoparticles demonstrated a substantially increased stability at both 4 and 25 °C over 30 days. Particles showed an encapsulation efficiency of ≈64% and a pH-dependent behavior in which complete Tegafur release was extended over 168, 48 or 24 h at pH 7.4 (blood), 6.5 (extracellular microenvironment of tumors) or 5.5 (endosomes/lysosomes of tumor cells), respectively. Based on hemocompatibility and cell viability tests, chitosan-coated nanoparticles exhibited satisfactory biocompatibility and safety for drug delivery. Furthermore, Tegafur-loaded chitosan-decorated particles demonstrated enhanced anticancer efficiency, with half maximal inhibitory concentration values in HT-29 and T-84 cells of ≈ 4-fold and ≈3.5-fold less than that of the free drug and drug-loaded unmodified nanoparticles, respectively. *In vivo* studies are needed to fully assess their efficacy and safety.

1. Introduction

Colorectal cancer (CRC) recorded approximately two million new cases and around one million deaths (10% of global cancer incidence and cancer deaths) worldwide in 2020, making it the third most commonly diagnosed cancer and the second leading cause of cancer-related death globally [1]. These rising numbers of CRC incidences and deaths pose an increasing public health and a heavy financial burden worldwide, and is largely thought to be related to the shifting toward westernized lifestyle and diet and the associated rise in exposure to environmental risk factors [2,3].

Recent advances in understanding the progression of CRC and broadening the treatment options have helped to improve the overall survival [4]. While surgical resection is the standard therapeutic procedure in patients in early tumor stages, other treatments including radiation therapy and chemotherapy are often indicated. Among these chemotherapeutic agents, Tegafur (TGF), a prodrug of 5-Fluorouracil that belongs to the group of pyrimidine analogues, has been employed for the treatment of a variety cancer lesions including head and neck, breast and advanced gastric and colorectal cancers [5–7]. In clinic, TGF is often used in combination with other anticancer agents such as Gimeracil–Oteracil, or along with Uracil [8].

However, the therapeutic efficacy of TGF is limited by its nonuniform oral absorption, its short biological half-life and the development of multidrug resistance by malignant cells [9]. Subsequently, repeated administration of TGF at higher doses may be necessary which concurrently lead to serious side effects. To address these drawbacks, the formulation of TGF in a nano-based drug delivery system can alter the

original characteristics of drug molecules and bring along several qualities such as enhancing the drug bioavailability, extending its blood circulation time, prolonging its liberation from the nanoformulation as well as providing surface functionalization possibilities, resulting in enhanced selectivity and therapeutic efficacy and reduced side effects [10–15].

Among polymers used for the design of drug encapsulating nanoparticles (NPs), poly(ε-caprolactone) (PCL) has recently been under intense interest in the field of drug delivery. PCL is a biodegradable and non-toxic polymer approved by FDA (US Food and Drug Administration) for clinical applications [16]. It has been widely used to formulate NPs with high drug encapsulation capacity and enhanced bioavailability and targeting abilities [17]. In addition, PCL's hydrophobic nature and slow degradation make it particularly useful for sustained delivery. To improve the properties of the hydrophobic negatively charged surface, PCL NPs can be coated with a hydrophilic polymer such as chitosan (CS). CS is a natural, biodegradable, nontoxic polysaccharide that has been extensively used as a NP-surface coating leading to an enhancement in mucoadhesion and retention in the intestinal epithelium, stability of the loaded drug and cellular uptake, and a prolongation in drug release profile [18–20].

In the current study, we aimed to design and assess CS-surface modified PCL NPs encapsulating TGF for the treatment of CRC. Firstly, we formulated CS-coated PCL NPs loaded with TGF for colon cancer treatment. Secondly, we extensively characterized the obtained NPs in terms of diameter, electrophoretic characteristics, short-term stability, encapsulation efficiency, *in vitro* drug release and blood compatibility. Finally, we evaluated the NPs *in vitro* for their ability to improve the anticancer activity against colon cancer cells.

2. Materials and methods

2.1. Materials

TGF, low molecular weight (M_W) CS ($\approx$50–190 kDa, determined by viscosity measurement; polydispersity not determined by the laboratory; $\approx$75–85% deacetylated; 99% purity level), PCL (average $M_W \approx$ 14,000 Da determined by gel permeation chromatography), Kolliphor® P-188, 3-(4,5-dimethylthiazol-2-yl)-3,5-diphenyl tetrazolium bromide (MTT), $C_6H_8O_7$, NaOH, Dulbecco's modified eagle's medium (DMEM), phosphate buffered saline (PBS), bovine serum albumin (BSA; heat shock fraction, ≥98% purity level), fetal bovine serum (FBS), and Penicillin-Streptomycin solution (containing 10,000 U/mL of Penicillin and 10 mg/mL of Streptomycin) were purchased from Merck KGaA (Gernsheim, Germany). All chemicals used were of analytical quality and used as received without further purification. Water used in the experiments was deionized and filtered with a Milli-Q® Academic System (Millipore, Spain).

2.2. Synthesis of nanoparticles

2.2.1. Synthesis of poly(ε-caprolactone) nanoparticles

PCL NPs were synthesized using an interfacial polymer disposition method [21–23]. Briefly, an organic solution containing 140 mg of PCL dissolved in 7 mL of dichloromethane was poured, under mechanical stirring (1000 rpm), to 35 mL of an aqueous solution of Kolliphor® P-188 (0.5%, w/v). For the preparation of drug-loaded NPs, TGF (at a concentration of 10^{-5} to 10^{-3} M) was incorporated into the aqueous medium. The organic solvent was then entirely removed using a Rotavapor® (Rotavapor® R II, Büchi, Flawil, Switzerland) and the PCL NPs were obtained as an aqueous dispersion. Next, NPs were purified by centrifugation at 5000 rpm during 30 min (Centrifuge 5804; Eppendorf Ibérica S.L.U., Spain) and re-dispersion in water for several cycles, until the conductivity value of the supernatant was ≤10 µS/cm. The obtained pellet was re-dispersed in water using ultrasonication.

2.2.2. Synthesis of chitosan and chitosan-decorated poly(ε-caprolactone) nanoparticles

CS NPs and CS-coated PCL NPs were both prepared by a coacervation method [24–26]. An aqueous solution of CS was first prepared by progressive addition of 110 mg of the polymer to 30 mL acetic acid (2%, v/v) containing 0.5% (w/v) Kolliphor® P-188, under mechanical stirring (500 rpm). Then, the pH of this aqueous CS solution was adjusted to pH 4 by adding NaOH 1 M. In the case of CS-coated PCL NPs, 75 mg of PCL NPs was added to the previous solution and homogeneously dispersed under mechanical stirring (500 rpm). Next, 7.5 mL of an aqueous solution of Na_2SO_4 (20%, w/v) was added drop-wise under sonication (sonication output of 20%, and sonication time of 10 min; Branson Sonifier 450, Emerson Electric Co., USA) to produce the NPs. Purification of NPs was carried out by centrifugation at 5000 rpm during 30 min, and re-dispersion in water for several cycles, until the conductivity value of the supernatant was ≤10 µS/cm. The obtained pellet was re-dispersed in water using ultrasonication.

2.3. Nanoparticle characterization

2.3.1. Mean diameter, size distribution and surface electrical charge (zeta potential, ζ)

Mean diameter and size distribution (polydispersity index, PdI), and zeta potential (ζ) of the obtained NPs were measured using dynamic light scattering and laser Doppler electrophoresis, respectively (Zetasizer Nano-ZS, Malvern Instruments Ltd., Worcestershire, UK) at 25.0 ± 0.5 °C. Before measurement, the nanoformulations were properly diluted in water (1 mg NP/mL).

2.3.2. Transmission electron microscopy and elemental analyses

The CS shell on the NPs was characterized using high resolution transmission electron microscopy (HRTEM) (Titan G2 60–300 FEI microscope, Thermofisher Scientific Inc., USA; accelerating voltage: 300 kV). A dispersion of the NPs ($\approx$0.1%, w/v) was applied to formvar/carbon-coated copper microgrids and subsequently dried in a convection oven (25.0 ± 0.5 °C) (J P. Selecta, S.A., Spain). Elemental analysis was performed during these determinations [Bruker Nano GmbH energy dispersive X-ray (EDX) spectrometer, Germany].

2.3.3. Studying electrophoretic characteristics as a function of pH and ionic strength

A qualitatively assessment of the CS coating onto the PCL NPs was also performed by analyzing the influence of pH and ionic strength on the ζ of the NPs [27,28]. To examine the effect of pH, a range between pH 3 and 10 in the presence of 1 mM KNO_3 was employed. In addition, the impact of ionic strength was examined using different concentrations of KNO_3 at a constant pH of $\approx$6 [23,29,30].

2.4. Evaluation of short-term stability and interaction with human serum proteins

Short-term stability of an aqueous dispersion of the colloidal formulations (1 mg/mL, pH ≈ 6) was assessed at 4.0 ± 0.5 °C or 25.0 ± 0.5 °C. Size, PdI and ζ values of the NPs were recorded and compared over 30 days.

Particle interaction with human serum proteins for potential formation of a protein corona was investigated *in vitro*. PCL, and CS-coated PCL NPs were incubated in PBS containing BSA for 60 min, following a previously described procedure [25,31]. Subsequently, the size and PdI were determined using dynamic light scattering.

2.5. Measurement of Tegafur loading capacity

Determinations of antitumor agent loading capacity in the NPs were performed indirectly by measuring free TGF remaining in the supernatant after the centrifugation step in the NP fabrication process. Drug

concentration was determined by photometric measurements, at a wavelength of 271 nm (Lambda™ 25 UV/Vis spectrophotometer, PerkinElmer Inc., USA) [32].

To avoid possible contributions to the absorbance of sources other than TGF, the absorbance of the supernatant of blank NPs was subtracted. Finally, the drug content was expressed as encapsulation efficiency (EE%) and drug loading (DL%) according to Equations (1) and (2).

$$EE\% = \frac{total\ drug\ amount - unencapsulated\ drug\ amount}{total\ drug\ amount} \times 100 \quad (1)$$

$$DL\% = \frac{total\ drug\ amount - unencapsulated\ drug\ amount}{total\ mass\ of\ NPs} \times 100 \quad (2)$$

2.6. In vitro release of Tegafur from nanoparticles

Drug release determinations from the CS-decorated PCL NPs was observed in buffers at different pH values. $C_6H_8O_7$–NaOH buffers at pH 5.5 ± 0.1 (pH of endosomes and lysosomes of tumor cells), pH 6.5 ± 0.1 (pH of extracellular microenvironment of tumors) and pH 7.4 ± 0.1 (blood pH) were prepared. The colloidal particles (1.5 g) were dispersed in 10 mL of each buffer. Throughout the experiment, dispersions were maintained at 37.0 ± 0.5 °C and under mechanical stirring (100 rpm). Aliquots (1 mL) of the buffer were sampled at selected time intervals, centrifuged at 11,000 rpm during 3 min, and the drug release was determined. After each sampling, an equal volume of the buffer, maintained at the same temperature, was pipetted to maintain the volume of the release medium and ensure sink conditions. Finally, the amount of released TGF was analyzed by measuring the optical absorbance at 271 nm. The results were expressed as a cumulative drug release percentage (Equation (3)).

$$Cumulative\ drug\ release\ (\%) = \frac{amount\ of\ TGF\ released\ in\ the\ medium\ (mg)}{amount\ of\ TGF\ loaded\ in\ the\ NPs\ (mg)}$$
$$\times 100$$
$$(3)$$

2.7. Ex vivo blood compatibility

Blood compatibility of the produced NPs was investigated to assess their suitability for *in vivo* administration. Human blood was obtained from healthy donors and poured into tubes containing either ethyleneaminetetraacetic acid (EDTA, used in the hemolysis and platelet activation experiments) or sodium citrate (used in the complement system activation and plasma recalcification time experiments) and treated following a previously established procedure [33–35]. NPs were incubated with blood aliquots to evaluate their effect on erythrocyte lysis (hemoglobin release), complement activation (C3a release), platelet activation (sP-selectin release) and plasma recalcification time ($T_{1/2\ max}$). Validated UV–vis spectrophotometric methodologies were employed. PBS served as a negative control.

2.8. In vitro cell culture experiments

2.8.1. Cell maintenance
Human cancer HT-29 (human colonic adenocarcinoma cells) and T-84 (human colon carcinoma cells) cell lines (American Type Culture Collection, ATCC, USA) were cultured in DMEM containing 10% FBS and 1% Penicillin-Streptomycin solution, and maintained until use at 37.0 ± 0.5 °C in a humidified 5% CO_2 incubator.

2.8.2. Cell viability assay
Treatments with various concentrations of TGF formulations dissolved/dispersed in the culture medium were added to cells and incubated for 72 h. Next, MTT (20 μL/well; 5 mg/mL in cell culture medium)

was added and incubation continued for 3 h at 37.0 ± 0.5 °C. Consequently, the culture medium was removed and the resulting formazan was dissolved with 200 μL of DMSO. Untreated cells and cells treated with Triton® X-100 1% served as controls. Finally, the optical density (OD) was measured at 570 nm using a Dynatech MR7000 microplate reader (Dynatech Laboratories, Inc., USA). The relative cell viability (RCV, %) was calculated as in Equation (4).

$$RCV\ (\%) = \frac{OD\ treated\ cells}{OD\ control\ (untreated)\ cells} \times 100 \quad (4)$$

The half maximal inhibitory concentration (IC_{50}) values were calculated from a non-linear regression analysis (GraphPad Prism 9.1.0, GraphPad Software Inc., La Jolla, CA, USA) [23,25,34].

2.9. Statistical analysis

All experiments were performed at least in three independent assays. The experimental data were expressed as mean value ± standard deviation (SD). The obtained data were subjected to statistical analysis performed using the SPSS Statistics 26 statistical package (IBM Corporation, USA). Groups of two were analyzed with two-tailed (Student's *t*-test, whereas groups greater than two with a single variable were compared using one-way analysis of variance (ANOVA), with Tukey's post-hoc test. The level of significance was set at $p < 0.05$.

3. Results

3.1. Nanoparticle characterization

The properties of PCL-based NPs are demonstrated in Table 1 (time 0). While the mean diameter of PCL NPs was 217.2 ± 5.1 nm, it was remarkably increased when NPs were surface coated with CS to 582.9 ± 51.4 nm. In addition, the PdI also increased from 0.232 ± 0.021 to 0.378 ± 0.061 for unmodified and coated NPs, respectively. Furthermore, the

Table 1
Mean diameter (nm), PdI, and ζ data (mV) of PCL and CS-decorated PCL particles as a function of time (days) at 4.0 ± 0.5 °C or 25.0 ± 0.5 °C. Experimental values are indicated as means ± SDs ($n = 3$).

Short-term stability assay at 25.0 ± 0.5 °C						
Time (days)	PCL NPs			CS-decorated PCL NPs		
	Size (nm)	PdI	ζ (mV)	Size (nm)	PdI	ζ (mV)
0	217.2 ± 5.1	0.232 ± 0.021	−15.13 ± 0.21	582.9 ± 51.4	0.378 ± 0.061	17.49 ± 0.24
1	196.1 ± 4.6	0.188 ± 0.011	−13.81 ± 0.15	582.2 ± 41.6	0.389 ± 0.021	16.94 ± 0.73
7	453.6 ± 35.7	0.499 ± 0.021	−6.92 ± 1.31	652.9 ± 97.3	0.491 ± 0.071	14.18 ± 0.88
14	439.5 ± 58.1	0.483 ± 0.061	−6.43 ± 0.85	645.1 ± 109.1	0.515 ± 0.031	14.88 ± 1.24
30	566.6 ± 48.5	0.555 ± 0.131	−4.51 ± 0.18	707.3 ± 22.1	0.511 ± 0.131	13.64 ± 0.13

Short-term stability assay at 4.0 ± 0.5 °C						
Time (days)	PCL NPs			CS-decorated PCL NPs		
	Size (nm)	PdI	ζ (mV)	Size (nm)	PdI	ζ (mV)
0	217.2 ± 5.1	0.232 ± 0.021	−15.13 ± 0.21	582.9 ± 51.4	0.378 ± 0.061	17.49 ± 0.24
1	231.4 ± 5.2	0.251 ± 0.031	−16.06 ± 0.71	601.5 ± 12.7	0.417 ± 0.021	15.26 ± 0.79
7	627.8 ± 173.1	0.609 ± 0.031	−7.01 ± 0.81	632.7 ± 66.2	0.457 ± 0.081	15.13 ± 0.62
14	731.9 ± 79.1	0.588 ± 0.211	−7.34 ± 1.63	684.5 ± 31.1	0.611 ± 0.031	14.25 ± 1.02
30	1229.1 ± 153.3	0.508 ± 0.021	−3.66 ± 1.33	628.3 ± 99.1	0.651 ± 0.061	15.39 ± 1.21

negative ζ of PCL NPs (- 15.1 $\pm$ 0.2 mV) was reversed to positive by coating with CS (+17.5 $\pm$ 0.2 mV). This change in ζ confirms that CS successfully coated the PCL NP surface and effectively shielded its negative charge, conferring a positive surface charge owing to its amine groups.

HRTEM characterization revealed the coating of PCL particles with a CS shell (Fig. 1a). Additionally, the EDX N element mapping of these core/shell particles suggested a uniform distribution of CS onto the PCL NPs (Fig. 1b). It should be noted that the particle aggregation observed in the Figure may have resulted from the sample preparation procedure for HRTEM observations, particularly during the drying process [24].

3.2. Studying electrophoretic characteristics as a function of pH and ionic strength

Variations in the electrophoretic characteristics of unmodified and CS-coated PCL NPs as a function of pH and ionic strength (KNO$_3$molar concentration) can be also employed to determine the efficiency of the method used for surface coating of the NPs (Fig. 2).

PCL NPs showed a slightly positive ζ at pH 3, which gradually decreased with an increase in pH, reaching approximately -30 mV at pH $\approx$ 9. However, when the concentration of KNO$_3$ was increased (at pH $\approx$ 6), the ζ of PCL NPs from around -20 mV at a concentration of 10^{-5} M to nearly a neutral value at a concentration of 10^{-2} M. On the other hand, CS-coated PCL NPs showed a positive ζ across the studied pH range (pH 3 to 9) (Fig. 2a), which was similar to that of CS NPs but relatively lower. While their ζ value was relatively stable at acidic pHs, lower values were measured at pH > 7. In addition, CS-coated PCL NPs were found to have a lower dependence on the ionic strength compared to PCL NPs, showing a similar trend to the control CS NPs (Fig. 2b).

3.3. Short-term stability and interaction with human serum proteins

Short-term stability at both 4 °C and 25 °C demonstrated a substantial improvement in the stability of NPs via the CS-surface modification (Table 1). Over the 30-day period of the experiment, unmodified NPs grew in size by $\approx$ 2.6-fold and $\approx$5.7-fold at 4 °C and 25 °C, respectively. Whereas, in the case of CS-coated NPs the changes were significantly lower with no more than $\approx$1.2-fold size increase at both conditions ($p < 0.05$). A similar trend was also observed with the PdI values. Furthermore, compared to the ζ of unmodified NPs which was increased by more than 10 mV at both conditions studied, the ζ of CS-decorated NPs was effectively maintained and only reduced by $\approx$ 3 mV over 30 days.

With reference to the interaction of the NPs with BSA, notable aggregation was observed for the unmodified PCL particles, resulting in a final diameter of 1313.6 $\pm$ 347.8 nm (PdI: 0.677 $\pm$ 0.037). In contrast, no significant effect on size was observed for the CS-coated NPs, with final particle size and PdI values of 591.3 $\pm$ 48.2 nm and 0.373 $\pm$ 0.046, respectively.
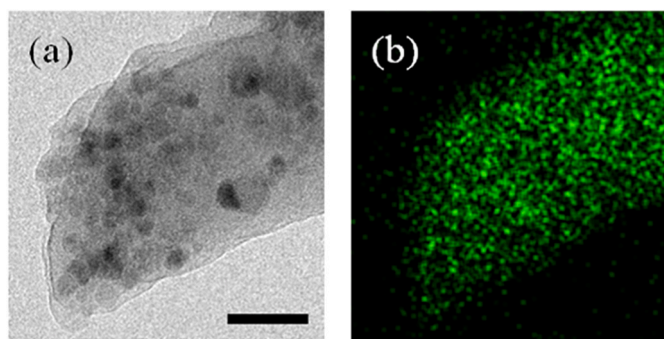

Fig. 2. Zeta potential (ζ, mV) of the PCL ($\bullet$), CS ($\blacksquare$), and CS-decorated PCL ($\circ$) particles as a function of: (*a*) pH in the presence of 1 mM KNO; and, (*b*) the KNO$_3$ molar concentration at pH $\approx$ 6. Data is given as mean value $\pm$ SD ($n = 9$).

3.4. Tegafur loading capacity

The EE (%) and DL (%) of TGF encapsulated in the CS-coated PCL NPs are collected in Table 2. As the drug concentration used in NP preparation was increased from 10^{-5} to 10^{-3} M, the EE (%) and DL (%) values increased substantially from around 11% and 0.0005% up to approximately 64% and 3%, respectively ($p < 0.05$).

3.5. In vitro release of Tegafur

The results of TGF release from CS-coated PCL NPs are plotted in Fig. 3. At pH 7.4, a clear biphasic profile was observed, where a rapid burst release of $\approx$30% of the TGF occurred within the first 6 h, while the remaining drug was released at a slower rate during the next 168 h. However, a substantially faster rate of drug release ($\approx$1.7-fold and $\approx$ 2-

Fig. 1. (*a*) HRTEM of the CS-decorated PCL particles; and, (*b*) EDX mapping analysis of the N element in sample (*a*). Bar length: 100 nm.
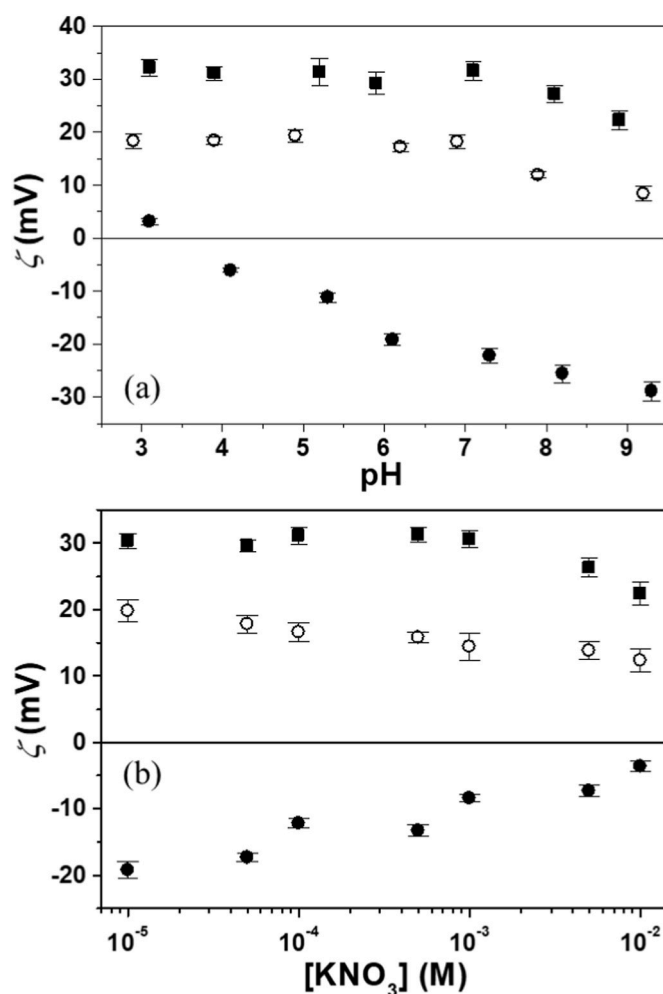
Table 2
Loading of Tegafur (EE and DL, %) to the CS-decorated PCL particles. Experimental values are indicated as means $\pm$ SDs ($n = 3$).

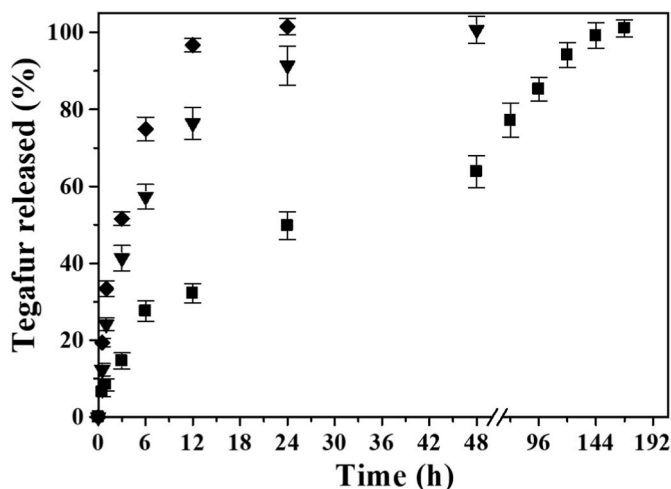| [Tegafur] (M)	EE (%)	DL (%)
10^{-5}	11.42 $\pm$ 1.17	0.0005 $\pm$ 0.0001
5×10^{-5}	17.32 $\pm$ 2.21	0.7578 $\pm$ 0.0967
10^{-4}	26.41 $\pm$ 2.04	1.1555 $\pm$ 0.0892
5×10^{-4}	42.19 $\pm$ 3.09	1.8459 $\pm$ 0.1352
10^{-3}	64.04 $\pm$ 2.36	2.8019 $\pm$ 0.1033

Fig. 3. Release of Tegafur (%) from the CS-decorated PCL particles as a function of the incubation time (h) at 37.0 ± 0.5 °C and pH of the bloodstream (pH 7.4 ± 0.1, ■), acidic extracellular microenvironment of tumors (pH 6.5 ± 0.1, ▼), or acidic environment in the endosomes and lysosomes of tumor cells (pH 5.5 ± 0.1, ◆). Data is presented as mean value $\pm$ SD ($n = 3$).

fold) was observed at pH 6.5 and 5.5 with 100% drug release achieved within only 48 and 24 h, respectively ($p < 0.05$).

3.6. Blood compatibility

Results of hemocompatibility tests performed on blank NPs (unloaded with drug) are presented in Table 3. CS-decorated NPs produced a negligible erythrolytic effect even after incubation for 24 h (only approximately 2%). In addition, the analysis of complement system activation, platelet activation plasma and clotting times demonstrated that the developed NPs did not significantly affect the levels of C3a and sP-selectin and $T_{1/2 \text{ max}}$.

3.7. In vitro cytotoxicity

As shown in Fig. 4, a negligible cytotoxicity by blank (drug-unloaded) CS-coated PCL NPs was produced in normal (CCD-18) and tumor (HT-29 and T-84) human cell lines over a wide range of concentrations.

Fig. 5, however, displays the cytotoxic effect of free TGF and drug-loaded NPs in HT-29 and T-84 cells following incubation for 72 h. These formulations inhibited cell proliferation in a dose-dependent manner. In both cell lines, the IC_{50} values of TGF-loaded CS-coated PCL NPs were $\approx$ 4-fold and $\approx$3.5-fold less than that of the free drug and drug-loaded unmodified NPs, respectively ($p < 0.05$). Whereas, effects

Table 3
Effects of the CS-decorated PCL particles NPs on hemolysis (%), complement activation (C3a release: C3a desArg, ng/mL), platelet activation (sP-selectin release, ng/mL), and plasma recalcification time ($T_{1/2 \text{ max}}$, min). Data is expressed as means $\pm$ SDs ($n = 3$).

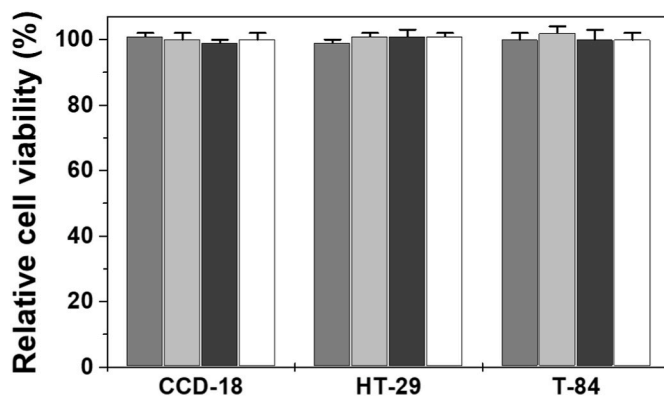|		CS-decorated PCL NPs	Control (PBS solution)
Hemolisis (%)	Incubation time: 2 h	2.1 ± 0.4	0
	Incubation time: 6 h	1.9 ± 0.5	0
	Incubation time: 12 h	2.3 ± 0.4	0
	Incubation time: 24 h	2.4 ± 0.3	0
C3a desArg (ng/mL)		303 ± 4	296 ± 5
sP-selectin release (ng/mL)		108 ± 7	99 ± 6
$T_{1/2 \text{ max}}$ (min)		13.6 ± 1.8	11.7 ± 1.4

Fig. 4. *In vitro* cytotoxicity of the CS-decorated PCL NPs in CCD-18 human colon fibroblast cells, and HT-29 and T-84 human colon cancer cells, after 72 h of exposure to a wide range of NP concentrations: 0.1 μM (grey column), 50 μM (light grey column), 100 μM (black column), and 200 μM (white column). The values are the mean $\pm$ standard deviation (SD) ($n = 4$). Cells without treatment were used as control to calculate the relative cell viability (%).
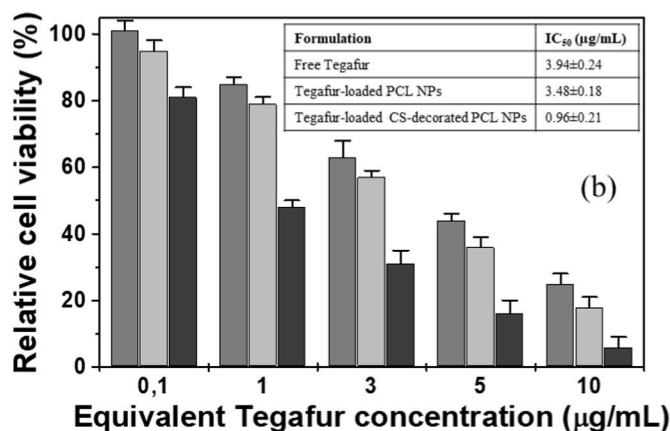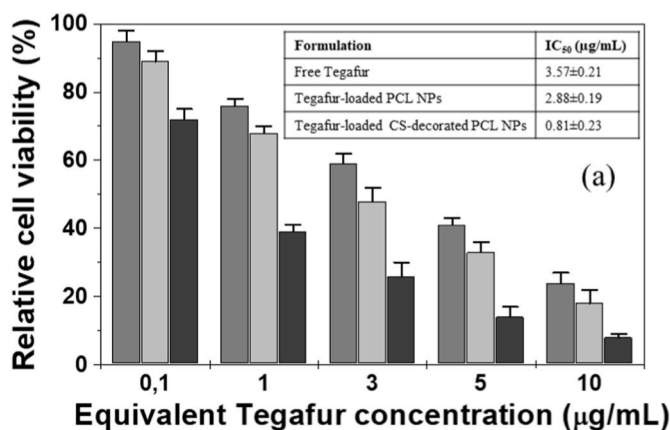

Fig. 5. Cytotoxicity of free Tegafur (grey column), Tegafur-loaded PCL NPs (light grey column), and Tegafur-loaded CS-decorated PCL NPs (black column) in HT-29 (a) and T-84 (b) human colon cancer cells, after 72 h of exposure to a wide range of NP concentrations (up to 10 μg/mL equivalent drug concentration). The values are the mean $\pm$ standard deviation (SD) ($n = 4$). Cells without treatment were used as control to calculate the relative cell viability (%). Inset: IC_{50} values (μM) of the Tegafur-based formulations.

of unmodified PCL NPs on cell viability were similar to those of the free antitumor agent at the concentrations used in both cell lines.

4. Discussion

In the current work, the formulation of PCL NPs surface functionalized with CS is described. The NPs loaded with the chemotherapeutic TGF were extensively characterized and examined *in vitro* for their suitability as a drug delivery system for the management of CRC.

The introduction of a cationic CS coat on PCL NPs brings about substantial changes to their surface charge and nature. This is manifested in the induced positive electrical charge to the NPs as well as their remarkably improved stability, as evidenced by the 30-day stability study at both 4 °C and 25 °C (Table 1). *In vitro* experiments examining the interaction of the NPs with BSA also indicated the protective effect of the hydrophilic CS coating onto the PCL particles, which could minimize protein corona formation and NP aggregation [25,36]. Incorporating CS during the process of NP preparation [37] or adding it to the surface of previously fabricated PCL NPs [38,39] are two strategies commonly utilized to perform the CS coat. In the latter, which was the chosen strategy, CS tends to adsorb to the surface of negatively-charged NPs driven by its cationic charge and the NP's high surface energy. This leads to the formation of a multi-layered coating [40].

The positive surface charge imparted by the CS prevents particles from aggregating due to the electrostatic repulsion created by this charge. This, in turn, helps maintain their physical stability when in aqueous dispersion. In biological settings, positively charged NPs show ability to interact with the negatively charged mucus and cells, leading to improved permeation, absorption and bioavailability of the NPs and their cargo. In addition, the mucoadhesive properties demonstrated by CS-coated NPs provide a longer residence time at the site, leading to an extended drug action. Finally, CS-coated PCL NPs demonstrated a relatively high entrapment efficiency of more than 60% (Table 2), indicating their efficacy in the encapsulation of TGF. Comparable loading capacity values have been previously described for PCL NPs loaded with various active ingredients [19,21–23,39].

In the electrophoretic characteristics study (Fig. 2), unmodified PCL NPs presented negative ζ due to the dissociation of the free acrylic groups (pKa 4.25) of the polymer, which occurs at higher extent with increasing pH values. In addition, the increased ζ associated with increasing the concentration of the electrolyte typically results from the classical double-layer compression mechanism, which is due to the increased ionic strength [35]. On the other hand, CS-coated NPs showed a similar behavior to the control CS NPs: a lower dependence on the ionic strength compared to PCL NPs and a positive charge which was reduced at pH > 7. This is because the cationic amine groups of CS have a pKa of 6.5, and therefor they become less protonated at basic pH values. These data suggest that PCL NPs were successfully coated with CS, which is further supported by the findings from transmission electron microscopy and elemental analyses (Fig. 1).

TGF release profile from CS-coated PCL NPs showed a biphasic behavior, which is characteristic of PCL NPs (Fig. 3) [21,41]. The initial burst of drug release is typically attributed to the instantaneous diffusion of molecules with weaker binding to the NP's surface. Subsequently, as polymer degradation/erosion progresses, mainly by hydrolysis, the drug embedded in the NP matrix continues to be released but at a slower rate. In addition, the CS coat may impose an additional limiting barrier for drug release, which is governed by factors such as the coat's thickness, the swelling and ionization of the polymer and drug diffusion through the polymeric matrix [19,42–44]. By examining release profiles at different pH values, it could be concluded that pH plays a crucial role in the release of TGF from CS-decorated PCL NPs. One significant advantage of this pH-dependent behavior is that the slow release observed at the physiological pH (pH 7.4) may reduce the presence of free drug in the bloodstream, hence, preventing its rapid clearance and non-specific

distribution. In contrast, the faster release rate observed at the pH of the extracellular microenvironment of tumors (pH 6.5) and the pH of endosomes and lysosomes of tumor cells (pH 5.5) is of particular interest for cancer treatment. It suggests that the nanosystem can facilitate the release of the drug at the tumor interstitium and to a larger extent upon internalization by tumor cells. These results are consistent with a previous study describing pH-responsive drug release features by non-coated PCL NPs loaded with Gemcitabine [23]. Another factor that may also contribute to this pH-dependent release is the role of the hydrophilic CS coat. CS (pKa 6.5) has its amine groups ionized in acidic solutions and, thus, it is more soluble at lower pH which in return can increase the wettability of the PCL matrix and result in an increase in drug diffusion and liberation [45,46].

Based on the data generated from blood compatibility tests (see Section 3.6.) and *in vitro* cell viability (see Section 3.7.) concerning the unloaded (drug free) CS-coated PCL NPs, it can be concluded that these polymeric nanocarriers exhibit satisfactory biocompatibility and safety for drug delivery purposes. Data showed a greater cytotoxicity against cancer cells with coated drug-loaded NPs compared to unmodified NPs and free drug. The superior results demonstrated by the CS-coated NPs are consistent with previous studies [19,38,47]. These studies found that the enhanced anticancer efficiency is associated with increased uptake of NPs by cancer cells. This increased uptake is believed to be facilitated by the improved interactions between the positively charged CS-decorated PCL particles and the negatively charged cellular membrane.

In addition to their potential use via various routes of administration, the developed CS-coated PCL NPs may also be useful for the oral route. Their relatively large size could facilitate passage through the gastrointestinal tract, while the CS coating could promote adhesion of the NPs to the mucus surface. Additionally, the enzymatic glycosidic linkage cleavage mediated by the colonic microflora may favor higher release at the colon [48].

5. Conclusions

In this work, it is described a reproducible procedure to prepare TFG-loaded CS-coated PCL-based NPs with a relatively high loading capacity. These NPs were examined *in vitro* and demonstrated improved stability, extended pH-dependent drug release profile, good biocompatibility and an enhanced anticancer efficiency against colorectal cells. While the developed NPs have shown promising results in *in vitro* studies using cell cultures, further research is needed to understand how these NPs will interact with the human body and affect treatments. *In vivo* studies are essential to fully assess the efficacy of this nanoformulation and ensure its safety.

Author statement

Ana Medina-Moreno: data curation, formal analysis, investigation, methodology.

Mazen M. El-Hammadi: formal analysis, validation, writing - original draft, writing - review & editing.

José L. Arias: conceptualization, data curation, investigation, methodology, supervision, validation, writing - review & editing.

Declaration of competing interest

None.

Data availability

Data will be made available on request.

Acknowledgements

References

[1] Y. Xi, P. Xu, Global colorectal cancer burden in 2020 and projections to 2040, Transl, Oncol. 14 (2021), 101174.

[2] N. Keum, E. Giovannucci, Global burden of colorectal cancer: emerging trends, risk factors and prevention strategies, Nat. Rev. Gastroenterol. Hepatol. 16 (2019) 713–732.

[3] N. Murphy, V. Moreno, D.J. Hughes, L. Vodicka, P. Vodicka, E.K. Aglago, M. J. Gunter, M. Jenab, Lifestyle and dietary environmental factors in colorectal cancer susceptibility, Mol. Aspect. Med. 69 (2019) 2–9.

[4] E. Dekker, P.J. Tanis, J.L.A. Vleugels, P.M. Kasi, M.B. Wallace, Colorectal cancer, Lancet 394 (2019) 1467–1480.

[5] T. Hata, K. Hagihara, A. Tsutsui, H. Akamatsu, T. Ohue, T. Shingai, M. Tei, M. Ikenaga, H.M. Kim, H. Osawa, H. Takemoto, K. Konishi, M. Uemura, C. Matsuda, T. Mizushima, K. Murata, Y. Ohno, Y. Doki, H. Eguchi, Administration method of adjuvant Tegafur-uracil and leucovorin calcium in patients with resected colorectal cancer: a phase III study, Oncol. 26 (2021) e735–e741.

[6] W. Li, X. Zhao, H. Wang, X. Liu, X. Zhao, M. Huang, L. Qiu, W. Zhang, Z. Chen, W. Guo, J. Li, X. Zhu, Maintenance treatment of Uracil and Tegafur (UFT) in responders following first-line fluorouracil-based chemotherapy in metastatic gastric cancer: a randomized phase II study, Oncotarget 8 (2017) 37826–37834.

[7] C. Li, T. Tang, W. Wang, Combination use of Tegafur and Apatinib as first-line therapy in treatment of advanced gastric cancer: a single-blinded randomized study, Gastroenterol. Res. Pract. 2020 (2020), 3232950.

[8] T. Watanabe, Evidence produced in Japan: tegafur-based preparations for postoperative chemotherapy in breast cancer, Breast Cancer 20 (2013) 302–309.

[9] M. Shahabi, H. Raissi, Screening of the structural, topological, and electronic properties of the functionalized Graphene nanosheets as potential Tegafur anticancer drug carriers using DFT method, J. Biomol. Struct. Dyn. 36 (2018) 2517–2529.

[10] J.L. Arias, M. López-Viota, V. Gallardo, M. Adolfina Ruiz, Chitosan nanoparticles as a new delivery system for the chemotherapy agent tegafur, Drug Dev. Ind. Pharm. 36 (2010) 744–750.

[11] J.L. Arias, E. Sáez-Fernández, M. López-Viota, R.A. Biedma-Ortiz, M.A. Ruiz, Synthesis of a biodegradable magnetic nanomedicine based on the antitumor molecule tegafur, Med. Chem. 8 (2012) 516–523.

[12] M.M. El-Hammadi, A.L. Small-Howard, M. Fernández-Arévalo, L. Martín-Banderas, Development of enhanced drug delivery vehicles for three cannabis-based terpenes using poly(lactic-co-glycolic acid) based nanoparticles, Ind. Crop. Prod. 164 (2021) 113345.

[13] M.M. El-Hammadi, A.L. Small-Howard, C. Jansen, M. Fernández-Arévalo, H. Turner, L. Martín-Banderas, Potential use for chronic pain: poly(ethylene glycol)-poly(lactic-co-glycolic acid) nanoparticles enhance the effects of cannabis-based terpenes on calcium influx in TRPV1-expressing cells, Int. J. Pharm. 616 (2022), 121524.

[14] M. López-Viota, M.M. El-Hammadi, L. Cabeza, J. Prados, C. Melguizo, M.A. Ruiz Martinez, J.L. Arias, Á.V. Delgado, Development and characterization of magnetite/poly(butylcyanoacrylate) nanoparticles for magnetic targeted delivery of cancer drugs, AAPS PharmSciTech 18 (2017) 3042–3052.

[15] R. Rebollo, F. Oyoun, Y. Corvis, M.M. El-Hammadi, B. Saubamea, K. Andrieux, N. Mignet, K. Alhareth, Microfluidic manufacturing of liposomes: development and optimization by design of experiment and machine learning, ACS Appl. Mater. Interfaces 14 (2022) 39736–39745.

[16] S. Witt, T. Scheper, J.G. Walter, Production of polycaprolactone nanoparticles with hydrodynamic diameters below 100 nm, Eng. Life Sci. 19 (2019) 658–665.

[17] W. Badri, K. Miladi, S. Robin, C. Viennet, Q.A. Nazari, G. Agusti, H. Fessi, A. Elaissari, Polycaprolactone based nanoparticles loaded with indomethacin for anti-inflammatory therapy: from preparation to ex vivo study, Pharm. Res. (N. Y.) 34 (2017) 1773–1783.

[18] M.K. Anwer, E.A. Ali, M. Iqbal, M.M. Ahmed, M.F. Aldawsari, A.A. Saqr, A. Alalaiwe, G.A. Soliman, Development of chitosan-coated PLGA-based nanoparticles for improved oral olaparib delivery: in vitro characterization, and in vivo pharmacokinetic studies, Processes 10 (2022) 1329.

[19] M.M. Badran, A.H. Alomrani, G.I. Harisa, A.E. Ashour, A. Kumar, A.E. Yassin, Novel docetaxel chitosan-coated PLGA/PCL nanoparticles with magnified cytotoxicity and bioavailability, Biomed. Pharmacother. 106 (2018) 1461–1468.

[20] S.S. Fong, Y.Y. Foo, W.S. Saw, B.F. Leo, Y.Y. Teo, I. Chung, B.T. Goh, M. Misran, T. Imae, C.C. Chang, L.Y. Chung, L.V. Kiew, Chitosan-coated-PLGA nanoparticles enhance the antitumor and antimigration activity of stattic - a STAT3 dimerization blocker, Int. J. Nanomed. 17 (2022) 137–150.

[21] J.L. Arias, M. López-Viota, E. Sáez-Fernández, M.A. Ruiz, Formulation and physicochemical characterization of poly(epsilon-caprolactone) nanoparticles loaded with ftorafur and diclofenac sodium, Colloids Surf. B Biointerfaces 75 (2010) 204–208.

[22] L. Cabeza, R. Ortiz, J. Prados, Á.V. Delgado, M.J. Martín-Villena, B. Clares, G. Perazzoli, J.M. Entrena, C. Melguizo, J.L. Arias, Improved antitumor activity and reduced toxicity of doxorubicin encapsulated in poly(epsilon-caprolactone) nanoparticles in lung and breast cancer treatment: an in vitro and in vivo study, Eur. J. Pharmaceut. Sci. 102 (2017) 24–34.

[23] G. García-García, F. Fernández-Álvarez, L. Cabeza, Á.V. Delgado, C. Melguizo, J. C. Prados, J.L. Arias, Gemcitabine-loaded magnetically responsive poly(epsilon-caprolactone) nanoparticles against breast cancer, Polymers 12 (2020) 2790.

[24] F. Fernández-Álvarez, C. Caro, G. García-García, M.L. García-Martín, J.L. Arias, Engineering of stealth (maghemite/PLGA)/chitosan (core/shell) shell nanocomposites with potential applications for combined MRI and hyperthermia against cancer, J. Mater. Chem. B 9 (2021) 4963–4980.

[25] F. Fernández-Álvarez, G. Garcia-Garcia, J.L. Arias, A tri-stimuli responsive (maghemite/PLGA)/chitosan nanostructure with promising applications in lung cancer, Pharmaceutics 13 (2021) 1232.

[26] Z. Sang, J. Qian, J. Han, X. Deng, J. Shen, G. Li, Y. Xie, Comparison of three water-soluble polyphosphate tripolyphosphate, phytic acid, and sodium hexametaphosphate as crosslinking agents in chitosan nanoparticle formulation, Carbohydr. Polym. 230 (2020), 115577.

[27] M. Moskvin, V. Huntosova, V. Herynek, P. Matous, A. Michalcova, V. Lobaz, B. Zasonska, R. Seliga, D. Horak, In vitro cellular activity of maghemite/cerium oxide magnetic nanoparticles with antioxidant properties, Colloids Surf. B Biointerfaces 204 (2021), 111824.

[28] R.C. Plaza, J.L. Arias, M. Espín, M.L. Jiménez, A.V. Delgado, Aging effects in the electrokinetics of colloidal iron oxides, J. Colloid Interface Sci. 245 (2002) 86–90.

[29] J.L. Arias, V. Gallardo, S.A. Gómez-Lopera, R.C. Plaza, A.V. Delgado, Synthesis and characterization of poly(ethyl-2-cyanoacrylate) nanoparticles with a magnetic core, J. Contr. Release 77 (2001) 309–321.

[30] J.L. Arias, V. Gallardo, F. Linares-Molinero, A.V. Delgado, Preparation and characterization of carbonyl iron/poly(butylcyanoacrylate) core/shell nanoparticles, J. Colloid Interface Sci. 299 (2006) 599–607.

[31] I. Russo Krauss, A. Picariello, G. Vitiello, A. De Santis, A. Koutsioubas, J. E. Houston, G. Fragneto, L. Paduano, Interaction with human serum proteins reveals biocompatibility of phosphocholine-functionalized SPIONs and formation of albumin-decorated nanoparticles, Langmuir 36 (2020) 8777–8791.

[32] J.L. Arias, M. Ruiz, V. Gallardo, A.V. Delgado, Tegafur loading and release properties of magnetite/poly(alkylcyanoacrylate) (core/shell) nanoparticles, J. Contr. Release 125 (2008) 50–58.

[33] B.C. Dash, G. Rethore, M. Monaghan, K. Fitzgerald, W. Gallagher, A. Pandit, The influence of size and charge of chitosan/polyglutamic acid hollow spheres on cellular internalization, viability and blood compatibility, Biomaterials 31 (2010) 8188–8197.

[34] M.M. El-Hammadi, Á.V. Delgado, C. Melguizo, J.C. Prados, J.L. Arias, Folic acid-decorated and PEGylated PLGA nanoparticles for improving the antitumour activity of 5-fluorouracil, Int. J. Pharm. 516 (2017) 61–70.

[35] M. Muñoz de Escalona, E. Sáez-Fernández, J.C. Prados, C. Melguizo, J.L. Arias, Magnetic solid lipid nanoparticles in hyperthermia against colon cancer, Int. J. Pharm. 504 (2016) 11–19.

[36] S.M. Pustulka, K. Ling, S.L. Pish, J.A. Champion, Protein nanoparticle charge and hydrophobicity govern protein corona and macrophage uptake, ACS Appl. Mater. Interfaces 12 (2020) 48284–48295.

[37] M.S. Shahab, M. Rizwanullah, S. Alshehri, S.S. Imam, Optimization to development of chitosan decorated polycaprolactone nanoparticles for improved ocular delivery of dorzolamide: in vitro, ex vivo and toxicity assessments, Int. J. Biol. Macromol. 163 (2020) 2392–2404.

[38] P. Huang, C. Yang, J. Liu, W. Wang, S. Guo, J. Li, Y. Sun, H. Dong, L. Deng, J. Zhang, J. Liu, A. Dong, Improving the oral delivery efficiency of anticancer drugs by chitosan coated polycaprolactone-grafted hyaluronic acid nanoparticles, J. Mater. Chem. B 2 (2014) 4021–4033.

[39] R. Vásquez Marcano, T.T. Tominaga, N.M. Khalil, L.S. Pedroso, R.M. Mainardes, Chitosan functionalized poly (epsilon-caprolactone) nanoparticles for amphotericin B delivery, Carbohydr. Polym. 202 (2018) 345–354.

[40] C. Guo, R.A. Gemeinhart, Understanding the adsorption mechanism of chitosan onto poly(lactide-co-glycolide) particles, Eur. J. Pharm. Biopharm. 70 (2008) 597–604.

[41] T.K. Dash, V.B. Konkimalla, Poly-ε-caprolactone based formulations for drug delivery and tissue engineering: a review, J. Contr. Release 158 (2012) 15–33.

[42] M. Dandamudi, P. McLoughlin, G. Behl, S. Rani, L. Coffey, A. Chauhan, D. Kent, L. Fitzhenry, Chitosan-coated PLGA nanoparticles encapsulating triamcinolone acetonide as a potential candidate for sustained ocular drug delivery, Pharmaceutics 13 (2021) 1590.

[43] M. Mohammed, H. Mansell, A. Shoker, K.M. Wasan, E.K. Wasan, Development and in vitro characterization of chitosan-coated polymeric nanoparticles for oral delivery and sustained release of the immunosuppressant drug mycophenolate mofetil, Drug Dev. Ind. Pharm. 45 (2019) 76–87.

[44] F. Yang, M. Cabe, H.A. Nowak, K.A. Langert, Chitosan/poly(lactic-co-glycolic)acid nanoparticle formulations with finely-tuned size distributions for enhanced mucoadhesion, Pharmaceutics 14 (2022) 95.

[45] M.M. Badran, M.M. Mady, M.M. Ghannam, F. Shakeel, Preparation and characterization of polymeric nanoparticles surface modified with chitosan for target treatment of colorectal cancer, Int. J. Biol. Macromol. 95 (2017) 643–649.

[46] M.A. Mohammed, J.T.M. Syeda, K.M. Wasan, E.K. Wasan, An overview of chitosan nanoparticles and its application in non-parenteral drug delivery, Pharmaceutics 9 (2017) 53.

[47] J.M. de Lima, L.R.C. Castellano, P.R.F. Bonan, E.S. de Medeiros, M. Hier, K. Bijian, M.A. Alaoui-Jamali, D.E. da Cruz Perez, S.D. da Silva, Chitosan/PCL nanoparticles can improve anti-neoplastic activity of 5-fluorouracil in head and neck cancer through autophagy activation, Int. J. Biochem. Cell Biol. 134 (2021), 105964.

[48] H. Choukaife, S. Seyam, B. Alallam, A.A. Doolaanea, M. Alfatama, Current advances in chitosan nanoparticles based oral drug delivery for colorectal cancer treatment, Int. J. Nanomed. 17 (2022) 3933–3966.